DTIC FILE (1)

①

REPORT DOCUMENTATION PAGE		READ INSTRUCTIONS BEFORE COMPLETING FORM
1. REPORT NUMBER AFIT/CI/NR 88-71	2. GOVT ACCESSION NO.	3. RECIPIENT'S CATALOG NUMBER
4. TITLE (and Subtitle) FINITE ELEMENT ANALYSIS OF SHELL STRUCTURES WITH AN EIGHTEEN-MODE THREE DIMENSIONAL SOLID ELEMENT BASED ON A NEW MIXED FORMULATION		5. TYPE OF REPORT & PERIOD COVERED MS THESIS
		6. PERFORMING ORG. REPORT NUMBER
7. AUTHOR(s) MICHAEL FREDERICK AUSSERER		8. CONTRACT OR GRANT NUMBER(s)
9. PERFORMING ORGANIZATION NAME AND ADDRESS AFIT STUDENT AT: UNIVERSITY OF MARYLAND		10. PROGRAM ELEMENT. PROJECT, TASK AREA & WORK UNIT NUMBERS
11. CONTROLLING OFFICE NAME AND ADDRESS		12. REPORT DATE 1988
		13. NUMBER OF PAGES 53
14. MONITORING AGENCY NAME & ADDRESS(if different from Controlling Office) AFIT/NR Wright-Patterson AFB OH 45433-6583		15. SECURITY CLASS. (of this report) UNCLASSIFIED
		15a. DECLASSIFICATION/DOWNGRADING SCHEDULE

AD-A196 698

16. DISTRIBUTION STATEMENT (of this Report)

DISTRIBUTED UNLIMITED: APPROVED FOR PUBLIC RELEASE

DTIC
ELECTE
AUG 0 3 1988
D

17. DISTRIBUTION STATEMENT (of the abstract entered in Block 20, if different from Report)

SAME AS REPORT

19. KEY WORDS (Continue on reverse side if necessary and identify by block number)

20. ABSTRACT (Continue on reverse side if necessary and identify by block number)
ATTACHED

DD FORM 1473 EDITION OF 1 NOV 65 IS OBSOLETE
1 JAN 73

UNCLASSIFIED

ABSTRACT

An eighteen-node, three-dimensional, solid element with 54 degrees of freedom is presented for the finite element analysis of thin plates and shells. The element is based on the Hellinger-Reissner principle with independent assumed strain. The independent strain is divided into higher and lower order terms. A modified stress-strain relation decoupling inplane and normal strain is used to model thin shell behavior. Numerical results demonstrate that this element is effectively free of locking even for very thin plates and shells. In addition, the element is kinematically stable. In fact, the stiffness matrix associated with the higher order independent strain is a stabilization matrix.

FINITE ELEMENT ANALYSIS OF SHELL STRUCTURES WITH AN

EIGHTEEN-NODE THREE DIMENSIONAL SOLID ELEMENT

BASED ON A NEW MIXED FORMULATION

by

Michael Frederick Ausserer

Thesis submitted to the Faculty of the Graduate School
of the University of Maryland in partial fulfillment
of the requirements for the degree of
Master of Science
1987

Advisory Committee:

Professor Inderjit Chopra
Associate Professor Sung. W. Lee
Assistant Professor Anthony Vizzini

ABSTRACT

Title of Thesis: Finite Element Analysis of Shell Structures with an Eighteen-Node, Three-Dimensional, Solid Element Based on a New Mixed Formulation

Michael Frederick Ausserer, Master of Science, 1987

Thesis Directed by: Dr. Sung W. Lee
                      Associate Professor
                      Department of Aerospace Engineering

An eighteen-node, three-dimensional, solid element with 54 degrees of freedom is presented for the finite element analysis of thin plates and shells. The element is based on the Hellinger-Reissner principle with independent assumed strain. The independent strain is divided into higher and lower order terms. A modified stress-strain relation decoupling inplane and normal strain is used to model thin shell behavior. Numerical results demonstrate that this element is effectively free of locking even for very thin plates and shells. In addition, the element is kinematically stable. In fact, the stiffness matrix associated with the higher order independent strain is a stabilization matrix.

ACKNOWLEDGMENTS

I would like to thank my advisor, Dr. Sung W. Lee, for his guidance and patience during the preparation of this thesis. Special thanks go to Dr. Jeong J. Rhiu and fellow graduate students too numerous to name for their invaluable assistance during my graduate program. Also, I would like to thank Dr. Inderjit Chopra and Dr. Anthony Vizzini for serving on the oral examining committee. Finally, and most importantly, I would like to thank my wife, Paula, for her constant encouragement and support.

TABLE OF CONTENTS

LIST OF FIGURES

LIST OF TABLES

LIST OF SYMBOLS

$\underset{\sim}{B}$ — Matrix relating local strain vector to element nodal degrees of freedom vector

$\underset{\sim}{\overline{B}}$ — Matrix relating lower order strain vector to element nodal degrees of freedom vector

$\underset{\sim}{B}^G$ — Matrix relating global strain vector to element nodal degrees of freedom vector

$\underset{\sim}{C}$ — Stress-strain relation

$\underset{\sim}{C}_m$ — Stress-strain relation modified for thin shell behavior

G — Shear modulus

$\underset{\sim}{G}, \underset{\sim}{H}$ — Matrices relating element strain parameters to element nodal degrees of freedom vector

$\underset{\sim}{K}$ — Global stiffness matrix

$\underset{\sim}{K}_e$ — Element stiffness matrix

$\underset{\sim}{K}_L$ — Element stiffness matrix for reduced integration of assumed displacement model

$\underset{\sim}{K}_S$ — Stabilization stiffness matrix

$\underset{\sim}{M}$ — Vector of shape function polynomials

N_i — Shape function at node i

$\tilde{N}_i$ — Trilinear shape function at node i

$\underset{\sim}{P}$ — Shape function matrix for higher order assumed strain

$\underset{\sim}{Q}$ — Global load vector

$\underset{\sim}{Q}_e$ — Element load vector

T — Transpose of a matrix

$\underset{\sim}{T}$	Transformation matrix relating global strain vector to local strain vector
$\underset{\sim}{U}$	Displacement vector in global coordinate system
$\underset{\sim}{V}_e$	Volume of an element
$\underset{\sim}{X}$	Position vector in global coordinate system
X, Y, Z	Global coordinates
$\underset{\sim}{a}_1, \underset{\sim}{a}_2, \underset{\sim}{a}_3$	Local orthogonal unit vectors
$\underset{\sim}{g}_e$	Element nodal degrees of freedom vector
$\underset{\sim}{v}_1, \underset{\sim}{v}_2$	Unit vectors at element centroid
x, y, z	Local coordinate system
θ	Angle between unit vectors at element centroid
$\underset{\sim}{\sum}$	Summation
$\underset{\sim}{\alpha}$	Element strain parameter vector
$\underset{\sim}{\varepsilon}$	Assumed independent strain vector
$\underset{\sim}{\bar{\varepsilon}}$	Local displacement-dependent strain vector
$\underset{\sim}{\bar{\varepsilon}}^G$	Global displacement-dependent strain vector
$\underset{\sim}{\varepsilon}_H$	Assumed higher order independent strain vector
$\underset{\sim}{\varepsilon}_L$	Assumed lower order independent strain vector
ν	Poisson's ratio
ξ, η, ζ	Parent coordinates

Chapter 1

INTRODUCTION

In recent years numerous finite element models based on the degenerate solid shell concept [1] have been proposed for the analysis of thin shell structures [2-4]. A distinct advantage of the degenerate solid shell concept is that it can be used for finite element modeling of arbitrary shell geometries without resorting to a specific shell theory. However, when used in an assumed displacement formulation, the performance of a degenerate solid shell element deteriorates rapidly as thickness decreases. This phenomenon is called locking and results from the inability of an element to represent a zero inplane and transverse strain state without disrupting the bending behavior [5].

One popular method used in an attempt to alleviate locking is reduced/selective integration [6-11]. However, reduced/selective integration has had limited success. In some elements the locking effect is not completely alleviated [12]. More commonly, when the order of integration is reduced sufficiently to alleviate locking, spurious kinematic or zero strain energy modes are introduced to the element stiffness matrix. These kinematic modes can be suppressed by adding a stabilization matrix to the stiffness matrix calculated using reduced integration [13,14].

An alternate method suggested by Lee and Pian [5] is to use a formulation with assumed independent strain based on the Hellinger-Reissner principle. A nine-node shell element based on this approach performed very well on a variety of thin shell test problems

1

[15]. This formulation provides a rational mathematical basis for the reduced integration scheme [5, 16, 17].

Recently, Rhiu and Lee successfully developed nine-node and sixteen-node degenerate solid shell elements using a new mixed formulation [3, 4] which is also based on the Hellinger-Reissner principle with independent strain. In this case, the assumed independent strain is divided into a higher order and a lower order part. The new mixed formulation provides a rational basis for introducing a stabilization matrix to the reduced integration displacement model.

Another approach to the finite element analysis of shell structures that also allows for the modeling of arbitrary geometries without invoking a specific shell theory is to use a three-dimensional, eighteen-node, solid element. In fact, a solid element is more convenient than a degenerate solid shell element since it does not need rotational angles to describe the kinematics of deformation.

However, when used in a conventional assumed displacement finite element formulation this eighteen-node element performs poorly. It experiences the same inplane and transverse shear locking that degenerate solid shell elements do. In addition, there is a normal strain locking due to the inability of the element to represent the condition of zero normal strain. The use of reduced integration results in spurious kinematic or zero strain energy modes in the finite element model. Hence, the global stiffness matrix may be kinematically unstable. Although many kinematically unstable elements can be used with care, they are of little value for general purpose use.

Therefore, in this study a new mixed formulation with assumed independent strain [12] is applied to the eighteen-node solid element to improve element performance. After a brief discussion of geometry and kinematics of deformation, a new mixed formulation for solid elements is presented. Next, the selection of assumed independent strain is discussed in detail. This is followed by a brief discussion on the modified stress-strain relation. Finally, the performance of the element is tested by solving several thin plate and shell problems.

Chapter 2

GEOMETRY AND KINEMATICS

Figure 1 shows the isoparametric representation of a three-dimensional, eighteen-node element. There are three displacement degrees of freedom at each node. Shape function polynomials are quadratic in parent coordinates ξ and η, and linear in ζ. The linear coordinate ζ is in the thickness direction of a thin structure.

In addition to a global Cartesian coordinate system with coordinates X, Y and Z, local orthogonal coordinate systems are used to incorporate shell behavior into the finite element formulation as will be shown later. In particular, local coordinate systems are defined at numerical integration points. This enables the use of the stress-strain relation as well as strain components defined with respect to the local coordinate system. For a local coordinate system, the three axes x, y and z are parallel to local orthogonal unit vectors $\underset{\sim}{a}_1$, $\underset{\sim}{a}_2$ and $\underset{\sim}{a}_3$, respectively. Local coordinate vector $\underset{\sim}{a}_1$ is chosen to be parallel with either ξ or η. These coordinate systems are chosen so that the element stiffness matrix is invariant for a given element geometry. The technique for choosing coordinate systems at integration points is discussed in detail later.

Given these coordinate systems, the position vector $\underset{\sim}{X}$ in the global coordinate system of an arbitrary point is

$$\underset{\sim}{X} = \left\{ \begin{array}{c} X \\ Y \\ Z \end{array} \right\} = \sum_{i=1}^{18} N_i(\xi,\eta,\zeta) \underset{\sim}{X}_i \tag{1}$$

4

where N_i is the three-dimensional Lagrange shape function at node i and $\underset{\sim}{X}_i$ are the values of $\underset{\sim}{X}$ at node i. Similarly, the global displacement vector $\underset{\sim}{U}$ of the same point is

$$\underset{\sim}{U} = \begin{Bmatrix} U \\ V \\ W \end{Bmatrix} = \sum_{i=1}^{18} N_i(\xi,\eta,\zeta)\underset{\sim}{U}_i \tag{2}$$

where $\underset{\sim}{U}_i$ is the vector of nodal displacements.

In matrix form, the linearized engineering strain vector $\overline{\underset{\sim}{\varepsilon}}^G$ with respect to global coordinates is

$$\overline{\underset{\sim}{\varepsilon}}^G = \begin{Bmatrix} U,_X \\ V,_Y \\ W,_Z \\ U,_Y + V,_X \\ V,_Z + W,_Y \\ U,_Z + W,_X \end{Bmatrix} \tag{3}$$

where the comma (,) denotes differentiation. For a finite element formulation, the relationship between $\overline{\underset{\sim}{\varepsilon}}^G$ and the nodal degrees of freedom vector $\underset{\sim}{g}_e$ can be written symbolically as

$$\overline{\underset{\sim}{\varepsilon}}^G = \underset{\sim}{B}^G \underset{\sim}{g}_e \tag{4}$$

where $\underset{\sim}{B}^G$ is a matrix relating $\overline{\underset{\sim}{\varepsilon}}^G$ to $\underset{\sim}{g}_e$. The strain vector in the local coordinate system is found by transforming the global strain vector as follows:

$$\overline{\underset{\sim}{\varepsilon}} = \underset{\sim}{T} \overline{\underset{\sim}{\varepsilon}}^G = \underset{\sim}{B} \underset{\sim}{g}_e \tag{5}$$

where

$$\underline{\bar{\varepsilon}} = \lfloor \bar{\varepsilon}_{xx} \; \bar{\varepsilon}_{yy} \; \bar{\varepsilon}_{zz} \; \bar{\varepsilon}_{xy} \; \bar{\varepsilon}_{yz} \; \bar{\varepsilon}_{zx} \rfloor^{T}$$

$$\underline{B} = \underline{T} \; \underline{B}^{G}$$

In Eq. (5) $\underline{T}$ is a 6x6 transformation matrix and the superscript T denotes the transpose.

Chapter 3

FINITE ELEMENT FORMULATION

Assuming small displacements and no initial strains (such as thermal strains), the functional π_R for the Hellinger-Reissner principle is

$$\pi_R = \sum \int_{V_e} (\underset{\sim}{\varepsilon}^T \, \underset{\sim}{C} \, \overline{\underset{\sim}{\varepsilon}} - \frac{1}{2} \underset{\sim}{\varepsilon}^T \, \underset{\sim}{C} \, \underset{\sim}{\varepsilon}) dV_e - W_o \qquad (6)$$

where

$$\underset{\sim}{\varepsilon} = \lfloor \varepsilon_{xx} \; \varepsilon_{yy} \; \varepsilon_{zz} \; \varepsilon_{xy} \; \varepsilon_{yz} \; \varepsilon_{zx} \rfloor^T \qquad (7)$$

is the independent strain vector, W_o is the applied load term, V_e is the volume of the element, $\underset{\sim}{C}$ is a 6x6 matrix of elastic coefficients and $\overline{\underset{\sim}{\varepsilon}}$ is the local strain vector derived from the displacement field given by Eq. (5). The summation sign indicates assembly of all elements.

As proposed in reference 12, the independent local strain vector is divided into two parts as follows:

$$\underset{\sim}{\varepsilon} = \underset{\sim}{\varepsilon}_L + \underset{\sim}{\varepsilon}_H \qquad (8)$$

where $\underset{\sim}{\varepsilon}_L$ and $\underset{\sim}{\varepsilon}_H$ are the independent, local strain vectors with lower order and higher order assumed polynomial terms in ξ, η and ζ, respectively. Substituting Eq. (8) into Eq. (6) and expanding yields the following functional:

7

$$\pi_R = \sum \left[\int \varepsilon_L^T \underset{\sim}{C} \, \bar{\varepsilon} \, dV_e - \frac{1}{2} \int \varepsilon^T \underset{\sim}{C} \, \varepsilon_L \, dV_e + \int \varepsilon_H^T \underset{\sim}{C} \, \bar{\varepsilon} \, dV_e \right.$$

$$\left. - \int \varepsilon_H^T \underset{\sim}{C} \, \varepsilon_L \, dV_e - \frac{1}{2} \int \varepsilon_H^T \underset{\sim}{C} \, \varepsilon_H \, dV_e \right] - W_0 \qquad (9)$$

In the present eighteen-node element the lower order independent strains are assumed to be trilinear in ξ, η and ζ. They are expressed in terms of displacement-dependent strains evaluated using a 2x2x2 point Gauss quadrature rule. Specifically,

$$\varepsilon_L = \sum_{i=1}^{8} \tilde{N}_i(\xi,\eta,\zeta) \bar{\varepsilon}_i = \sum_{i=1}^{8} \tilde{N}_i(\xi,\eta,\zeta) \underset{\sim}{B}(\xi_i,\eta_i,\zeta_i) q_e \qquad (10)$$

where $\tilde{N}_i$ is the trilinear shape function such that $\tilde{N}_i = 1$ at sampling point i of the 2x2x2 point integration rule, $\bar{\varepsilon}_i$ is displacement-dependent strain evaluated at sampling point i, and ξ_i, η_i, ζ_i are the values for ξ, η and ζ at sampling point i. Symbolically, the relation between ε_L and q_e is rewritten as

$$\varepsilon_L = \bar{B}(\xi,\eta,\zeta) q_e \qquad (11)$$

where

$$\bar{B}(\xi,\eta,\zeta) = \sum_{i=1}^{8} \tilde{N}_i(\xi,\eta,\zeta) \, \underset{\sim}{B}(\xi_i,\eta_i,\zeta_i)$$

The higher order strain vector is assumed to have higher order terms in ξ, η and ζ, and is written as

$$\varepsilon_H = \underset{\sim}{P}(\xi,\eta,\zeta) \, \underset{\sim}{\alpha} \qquad (12)$$

8

where $\underset{\sim}{P}$ is the shape function matrix of higher order assumed strains and $\underset{\sim}{\alpha}$ is a vector containing element strain parameters.

Introducing Eqs. (5), (11) and (12) into Eq. (9) yields the following expression:

$$\pi_R = \sum \left(\frac{1}{2} \underset{\sim}{q}_e^T \underset{\sim}{K}_L \underset{\sim}{q}_e + \underset{\sim}{\alpha}^T \underset{\sim}{G} \underset{\sim}{q}_e - \frac{1}{2} \underset{\sim}{\alpha}^T \underset{\sim}{H} \underset{\sim}{\alpha} - \underset{\sim}{q}_e^T \underset{\sim}{Q}_e \right) \qquad (12)$$

where

$$\underset{\sim}{K}_L = \int (\overline{\underset{\sim}{B}}^T \underset{\sim}{C} \underset{\sim}{B} + \underset{\sim}{B}^T \underset{\sim}{C} \overline{\underset{\sim}{B}} - \overline{\underset{\sim}{B}}^T \underset{\sim}{C} \overline{\underset{\sim}{B}}) \, dV_e \qquad (13a)$$

$$\underset{\sim}{G} = \int \underset{\sim}{P}^T \underset{\sim}{C} \underset{\sim}{B} \, dV_e - \int \underset{\sim}{P}^T \underset{\sim}{C} \overline{\underset{\sim}{B}} \, dV_e \qquad (13b)$$

$$\underset{\sim}{H} = \int \underset{\sim}{P}^T \underset{\sim}{C} \underset{\sim}{P} \, dV_e \qquad (13c)$$

and $\underset{\sim}{Q}_e$ is the element load vector.

Taking $\delta\pi_R = 0$ with respect to $\underset{\sim}{\alpha}$ for each element yields the following relationships:

$$\underset{\sim}{G} \underset{\sim}{q}_e - \underset{\sim}{H} \underset{\sim}{\alpha} = \underset{\sim}{0} \qquad (14a)$$

and

$$\underset{\sim}{\alpha} = \underset{\sim}{H}^{-1} \underset{\sim}{G} \underset{\sim}{q}_e \qquad (14b)$$

Equation (14a) or (14b) represents the compatibility equation for each element in discretized form. Using Eq. (14b) in Eq. (13) results in a familiar expression for π_R as follows:

$$\pi_R = \sum \left(\frac{1}{2} \underset{\sim}{q}_e^T \underset{\sim}{K}_e \underset{\sim}{q}_e - \underset{\sim}{q}_e^T \underset{\sim}{Q}_e \right) \qquad (15)$$

where the element stiffness matrix $\underset{\sim}{K}_e$ is given by

$$\underset{\sim}{K}_e = \underset{\sim}{K}_L + \underset{\sim}{K}_S \qquad (15a)$$

9

and the stabilization matrix $\underset{\sim}{K}_S$ is given by

$$\underset{\sim}{K}_S = \underset{\sim}{G}^T \underset{\sim}{H}^{-1} \underset{\sim}{G} \tag{15b}$$

After assembly over all elements, Eq. (15) can be rewritten as

$$\pi_R = \frac{1}{2} \underset{\sim}{g}^T \underset{\sim}{K} \underset{\sim}{g} - \underset{\sim}{g}^T \underset{\sim}{Q} \tag{16}$$

where $\underset{\sim}{K}$ is the global stiffness matrix, $\underset{\sim}{g}$ is the global displacement vector and $\underset{\sim}{Q}$ is the global load vector. Setting $\delta\pi_R = 0$ with respect to $\underset{\sim}{g}$ gives

$$\underset{\sim}{K} \underset{\sim}{g} = \underset{\sim}{Q} \tag{17}$$

which can be solved for $\underset{\sim}{g}$. Thus, $\underset{\sim}{g}_e$ is known, and the local strain vector is determined as follows:

$$\underset{\sim}{\varepsilon} = \underset{\sim}{\varepsilon}_L + \underset{\sim}{P} \underset{\sim}{H}^{-1} \underset{\sim}{G} \underset{\sim}{g}_e \tag{18a}$$

Stress $\underset{\sim}{\sigma}$ is determined by using the stress-strain relation and the strain in Eq. (18a) as follows:

$$\underset{\sim}{\sigma} = \underset{\sim}{C} \underset{\sim}{\varepsilon} \tag{18b}$$

As will be demonstrated in the next section the $\underset{\sim}{K}_L$ matrix in Eq. (13a) has spurious kinematic modes. The kinematic modes occur because only lower order terms of assumed strain are used in constructing $\underset{\sim}{K}_L$. When higher order assumed strain is properly chosen, the $\underset{\sim}{K}_S$ matrix plays the role of a stabilization matrix and the element stiffness matrix will be kinematically stable.

Before discussing the selection of higher order strain a few comments on numerically integrating the expressions for π_R in Eqs.

10

(13a-c) are in order. Since $\bar{\underset{\sim}{\epsilon}}$ is quadratic in ξ and η, and linear in ζ for an element with regular parallelepiped geometry, and $\underset{\sim}{\epsilon}_L$ is assumed to be trilinear, then Eq. (13a) is integrated exactly with a 2x2x2 point Gauss numerical integration rule. In this case Eq. (13a) reduces to

$$\underset{\sim}{K}_L = \int_L \underset{\sim}{B}^T \underset{\sim}{C} \underset{\sim}{B} \, dV_e \qquad (19)$$

where the subscript L on the integral sign indicates a 2x2x2 point integration rule. In other words, the $\underset{\sim}{K}_L$ matrix in Eq. (13a) is exactly the same as the stiffness matrix for the assumed displacement model with a 2x2x2 point reduced integration rule. Detailed discussions of the equivalence between reduced integration and mixed formulations are in references 12, 16 and 17. Assuming $\underset{\sim}{\epsilon}_H$ is at most quadratic in ξ and η, and linear in ζ, Eq. (13c) and the first integral in Eq. (13b) require a 3x3x2 point integration rule for exact integration of the same regularly shaped element. The second integral in Eq. (13b) is integrated exactly with a 2x2x2 point rule. Although these rules are only exact for an element with rectangular geometry, the same integration rules are adopted for elements with distorted geometries.

11

Chapter 4

HIGHER ORDER ASSUMED STRAIN

The critical step in the present formulation is the proper choice of assumed strain. Generally, the assumed strain should be as simple as possible to avoid locking. However, an exceedingly simple assumed strain field will trigger spurious kinematic modes that do not produce strain [3]. These kinematic modes are of two types; compatible and incompatible. Compatible kinematic modes persist even when two or more elements are assembled. In other words, compatible kinematic modes are modes that will show up in the global stiffness matrix. On the other hand, incompatible kinematic modes are suppressed when two or more elements are a sembled. Since incompatible kinematic modes have no adverse effect on the global stiffness matrix, assumed strain can be chosen to suppress only compatible kinematic modes in the element stiffness matrix. In addition, assumed strain terms must be chosen carefully in order to avoid reintroducing the locking effect.

4.1 Local Coordinate System

The typical result of choosing assumed strain as simple as possible is an incomplete set of shape function polynomials in $\underset{\sim}{P}$. In general, this leads to an element stiffness matrix which is not invariant. Although invariance is not always important, it can be enforced by assigning a specific local coordinate system for a given element geometry [18]. For an arbitrary thin element, two unit vectors $\underset{\sim}{v}_1$ and $\underset{\sim}{v}_2$ are defined at $\xi = \eta = \zeta = 0$ so that $\underset{\sim}{v}_1$ is parallel to ξ and $\underset{\sim}{v}_2$ is

parallel to n. The angle θ between $\underset{\sim}{v}_1$ and $\underset{\sim}{v}_2$ is given by

$$\theta = \cos^{-1} (\underset{\sim}{v}_1 \cdot \underset{\sim}{v}_2) \tag{20}$$

If θ is less than or equal to 90°, then the $\underset{\sim}{a}_1$ unit vector in the x
direction of the local coordinate system is chosen parallel with ξ.
Otherwise $\underset{\sim}{a}_1$ is chosen parallel to n. Next the $\underset{\sim}{a}_3$ vector normal to the
ξ-n plane is determined. Finally, unit vector $\underset{\sim}{a}_2$ is found by taking
the cross product between $\underset{\sim}{a}_3$ and $\underset{\sim}{a}_1$. Based on the value of θ for the
element, vectors $\underset{\sim}{a}_1$, $\underset{\sim}{a}_2$ and $\underset{\sim}{a}_3$ can be computed at any point in the
element. In particular, they are calculated at each numerical
integration point. This definition of $\underset{\sim}{a}_1$, $\underset{\sim}{a}_2$ and $\underset{\sim}{a}_3$ guarantees a
unique set of local coordinate systems for a given element geometry,
and thus a stiffness matrix independent of choice of global coordinate
system.

4.2 Spurious Kinematic Modes

As discussed in Chapter 3, the $\underset{\sim}{K}_L$ matrix in Eq. (13a) or (19) has
kinematic modes which can be suppressed with the proper choice of
higher order assumed strain. Thus, when $\underset{\sim}{P}$ is chosen properly, the $\underset{\sim}{K}_S$
matrix plays the role of a stabilization matrix. In fact, for the new
mixed formulation the higher order assumed strain is chosen specifi-
cally to suppress kinematic modes [12]. Therefore, the kinematic modes
must be known before the higher order strain terms are selected.

Kinematic modes for the $\underset{\sim}{K}_L$ matrix can be determined analytically
for an element with regular parallelepiped geometry. For a cubic
element with sides along x = ±1, y = ±1 and z = ±1 and the global and

13

local coordinate systems coincident, the displacement field can be written as

$$
\left\{ \begin{array}{c} U \\ V \\ W \end{array} \right\} = \left[\begin{array}{cccccc} a_1 & a_2 & a_3 & \cdot & \cdot & \cdot & a_{18} \\ b_1 & b_2 & b_3 & \cdot & \cdot & \cdot & b_{18} \\ c_1 & c_2 & c_3 & \cdot & \cdot & \cdot & c_{18} \end{array} \right] \underset{\sim}{M}
\tag{21}
$$

where

$$
\underset{\sim}{M} = \lfloor 1 \quad x \quad y \quad x^2 \quad xy \quad y^2 \quad x^2y \quad xy^2 \quad x^2y^2
$$
$$
z \quad zx \quad zy \quad zx^2 \quad zxy \quad zy^2 \quad zx^2y \quad zxy^2 \quad zx^2y^2 \rfloor^T
$$

The local displacement-dependent strain vector is determined by introducing Eq. (21) to Eq. (3). The displacement field corresponding to zero strain is found by setting the local strain vector equal to zero at the 2x2x2 integration points. Specifically,

$$
\overline{\underset{\sim}{\varepsilon}} \ (\pm 1/\sqrt{3}, \pm 1/\sqrt{3}, \pm 1/\sqrt{3}) = \underset{\sim}{0}
\tag{22}
$$

Equation (22) represents 48 homogeneous equations with 54 unknown variables. Solving these equations gives the following displacement field for zero strain:

$$
U = \underline{a_1 + a_3 y + a_{10} z} + a_2 x (1 - 3y^2) + a_4 (x^2 + y^2 - 3x^2 y^2)
$$
$$
+ a_{11} zx (1 - 3y^2) + a_{13} z (x^2 + y^2 - 3x^2 y^2)
\tag{23a}
$$

$$
V = \underline{b_1 - a_3 x + b_{10} z} - a_2 y (1 - 3x^2) + b_4 (x^2 + y^2 - 3x^2 y^2)
$$
$$
- a_{11} zy (1 - 3x^2) + b_{13} z (x^2 + y^2 - 3x^2 y^2)
\tag{23b}
$$

14

$$W = \underline{c_1 - a_{10}x - b_{10}y} - 1/3a_{13}x - 1/3b_{13}y$$

$$+ c_4(x^2 + y^2 - 3x^2y^2) + c_{10}z(1 - 3x^2 - 3y^2 + 9x^2y^2) \quad (23c)$$

The underlined terms in Eqs. (23a-c) are rigid body modes. The other terms represent spurious kinematic modes.

4.3 Assumed Strain

The strain terms corresponding to the kinematic modes in Eqs. (23a-c) are

$$\bar{\varepsilon}_{xx} = a_2(1 - 3y^2) + a_4(2x - 6xy^2) + a_{11}z(1 - 3y^2)$$
$$+ a_{13}z(2x - 6xy^2) \quad (24a)$$

$$\bar{\varepsilon}_{yy} = -a_2(1 - 3x^2) + b_4(2y - 6x^2y) - a_{11}z(1 - 3x^2)$$
$$+ b_{13}z(2y - 6x^2y) \quad (24b)$$

$$\bar{\varepsilon}_{zz} = c_{10}(1 - 3x^2 - 3y^2 + 9x^2y^2) \quad (24c)$$

$$\bar{\varepsilon}_{xy} = a_4(2y - 6x^2y) + b_4(2x - 6xy^2) + a_{13}z(2y - 6x^2y)$$
$$+ b_{13}z(2x - 6xy^2) \quad (24d)$$

$$\bar{\varepsilon}_{yz} = - a_{11}y(1 - 3x^2) + b_{13}(-\frac{1}{3} + x^2 + y^2 - 3x^2y^2)$$
$$+ c_4(2y - 6x^2y) + c_{10}z(- 6y + 18x^2y) \quad (24e)$$

$$\bar{\varepsilon}_{zx} = a_{11}x(1 - 3y^2) + a_{13}(-\frac{1}{3} + x^2 + y^2 - 3x^2y^2)$$
$$+ c_4(2x - 6xy^2) + c_{10}z(- 6x + 18xy^2) \quad (24f)$$

Higher order assumed strain terms are chosen by examining Eqs. (24a-f). For example, the kinematic mode represented by

15

$\bar{\varepsilon}_{xx} = a_4(2x-6xy^2)$ is suppressed if xy^2 is added to the higher order assumed strain shape functions for $(\varepsilon_{xx})_H$. Since the kinematic mode represented by a_4 can also be suppressed by including an x^2y term in $(\varepsilon_{xy})_H$, there must be a logical basis for deciding between the options. The general rule is to minimize the total number of terms in the assumed strain that contribute to locking. For a three-dimensional element applied to a thin structure this means that the polynomial terms independent of z (thickness) should be kept as simple as possible. Kinematic modes corresponding to a_2 and a_{11} need not be suppressed since they are incompatible and disappear for the assembly of two or more elements.

Even with the general rule there are still two reasonable alternate sets of higher order strain. One option is to minimize the total number of terms in the higher order strain field as follows:

$$(\varepsilon_{xx})_H = \alpha_1 xy^2 + \alpha_2 xy^2 z$$
$$(\varepsilon_{yy})_H = \alpha_3 x^2 y + \alpha_4 x^2 yz$$
$$(\varepsilon_{zz})_H = \alpha_5 x^2 y^2$$
$$(\varepsilon_{xy})_H = 0 \qquad\qquad (25)$$
$$(\varepsilon_{yz})_H = \alpha_6 x^2 y$$
$$(\varepsilon_{zx})_H = \alpha_7 xy^2$$

In Eq. (25), α_1, α_2, α_3, α_4, α_5, α_6, α_7 are unknown strain parameters. Note that only one term is needed between $(\varepsilon_{yz})_H$ and $(\varepsilon_{zx})_H$ to suppress the kinematic mode represented by c_4. The second term is added to avoid introducing a directional imbalance to the element stiffness

16

matrix. The model using this choice of assumed strain is designated New Mixed Solid, 18-node version, A (NMS18A).

The other alternative is to replace the x^2y^2 term in $(\varepsilon_{zz})_H$ with x^2yz and xy^2z terms in $(\varepsilon_{yz})_H$ and $(\varepsilon_{zx})_H$, respectively. Once again only one term is needed to suppress a kinematic mode (in this case c_{10}), but the second term is added to avoid introducing a directional imbalance. In this case, the total number of terms is increased by one to eight, but the new terms are expected to have a proportionally smaller effect as the thickness becomes smaller. This proposal is tested numerically in the next section. This formulation is designated NMS18B.

For completeness, all modes are suppressed by adding to the NMS18B version y^2 and y^2z terms to $(\varepsilon_{xx})_H$ and x^2 and x^2z terms to $(\varepsilon_{yy})_H$ to suppress the a_2 and a_{11} incompatible kinematic modes. As in the other formulations, only one term is needed to suppress each mode, but two terms are used to avoid introducing a directional imbalance. This formulation is designated NMS18C.

For an element with arbitrary geometry, ξ, η and ζ are used in place of x, y and z in Eq. (25). Therefore, with the local coordinate system defined previously, the higher order assumed strains for the eighteen-node solid element are chosen as follows:

$$\varepsilon_H = P\, \alpha \tag{26}$$

where for NMS18A

17

$$
\underset{\sim}{P} = \begin{bmatrix}
f & \zeta f & 0 & 0 & 0 & 0 & 0 & 0 \\
0 & 0 & g & \zeta g & 0 & 0 & 0 & 0 \\
0 & 0 & 0 & 0 & \xi^2 \eta^2 & 0 & 0 & 0 \\
0 & 0 & 0 & 0 & 0 & 0 & 0 & 0 \\
0 & 0 & 0 & 0 & 0 & 0 & g & 0 \\
0 & 0 & 0 & 0 & 0 & 0 & 0 & f
\end{bmatrix}
\tag{27a}
$$

$$
\underset{\sim}{\alpha}^T = \lfloor \alpha_1, \alpha_2, \alpha_3, \alpha_4, \alpha_5, \alpha_6, \alpha_7 \rfloor
\tag{27b}
$$

for NMS18B

$$
\underset{\sim}{P} = \begin{bmatrix}
f & \zeta f & 0 & 0 & 0 & 0 & 0 & 0 \\
0 & 0 & g & \zeta g & 0 & 0 & 0 & 0 \\
0 & 0 & 0 & 0 & 0 & 0 & 0 & 0 \\
0 & 0 & 0 & 0 & 0 & 0 & 0 & 0 \\
0 & 0 & 0 & 0 & g & \zeta g & 0 & 0 \\
0 & 0 & 0 & 0 & 0 & 0 & f & \zeta f
\end{bmatrix}
\tag{28a}
$$

$$
\underset{\sim}{\alpha}^T = \lfloor \alpha_1, \alpha_2, \alpha_3, \alpha_4, \alpha_5, \alpha_6, \alpha_7, \alpha_8 \rfloor
\tag{28b}
$$

18

and for NMS18C

$$
\underset{\sim}{P} =
\begin{bmatrix}
r & \zeta r & f & \zeta f & 0 & 0 & 0 & 0 \\
0 & 0 & 0 & 0 & s & \zeta s & g & \zeta g \\
0 & 0 & 0 & 0 & 0 & 0 & 0 & 0 \\
0 & 0 & 0 & 0 & 0 & 0 & 0 & 0 \\
0 & 0 & 0 & 0 & 0 & 0 & 0 & 0 \\
0 & 0 & 0 & 0 & 0 & 0 & 0 & 0
\end{bmatrix}
$$

$$
\begin{bmatrix}
0 & 0 & 0 & 0 \\
0 & 0 & 0 & 0 \\
0 & 0 & 0 & 0 \\
0 & 0 & 0 & 0 \\
g & \zeta g & 0 & 0 \\
0 & 0 & f & \zeta f
\end{bmatrix}
\tag{29a}
$$

$$
\underset{\sim}{a}^T = \lfloor \alpha_1, \alpha_2, \alpha_3, \alpha_4, \alpha_5, \alpha_6,
$$

$$
\alpha_7, \alpha_8, \alpha_9, \alpha_{10}, \alpha_{11}, \alpha_{12} \rfloor
\tag{29b}
$$

For Eqs. (27a), (28a) and (29a), f, g, h and i are chosen as follows:

(1)   if x or $\underset{\sim}{a}_1$ is parallel to ξ $(\theta < 90°)$

$$f = \xi n^2$$

$$g = \xi^2 n$$

$$r = n^2$$

$$s = \xi^2$$

(2)　　　if x or $\underset{\sim}{a}_1$ is parallel to n　　　$(\theta > 90°)$

$$f = \xi^2 n$$

$$g = \xi n^2$$

$$r = \xi^2$$

$$s = n^2$$

4.4 Modified Stress-Strain Relation

The stress-strain relation for an isotropic, three-dimensional solid can be modified to incorporate thin plate and shell behavior by assuming that first the effect of σ_{zz} on ε_{xx} and ε_{yy} is small and second the effect of σ_{xx} and σ_{yy} on ε_{zz} is small. Then

$$\varepsilon_{xx} = \frac{1}{E} (\sigma_{xx} - \nu\sigma_{yy}) \tag{30a}$$

$$\varepsilon_{yy} = \frac{1}{E} (\sigma_{yy} - \nu\sigma_{xx}) \tag{30b}$$

$$\varepsilon_{zz} = \frac{1}{E} \sigma_{zz} \tag{30c}$$

where E is Young's Modulus and ν is Poisson's ratio. The relations between shear strains and stresses remain unchanged as follows:

$$\varepsilon_{xy} = \frac{1}{G} \sigma_{xy} \tag{30d}$$

$$\varepsilon_{yz} = \frac{1}{G} \sigma_{yz} \tag{30e}$$

$$\varepsilon_{zx} = \frac{1}{G} \sigma_{zx} \tag{30f}$$

where G is the shear modulus.

Inverting Eqs. (30a-f) gives the modified stress-strain relation as follows:

$$\underset{\sim}{\sigma} = \underset{\sim}{C}_m \, \underset{\sim}{\varepsilon}$$

where

$$
\underset{\sim}{C}_m = \begin{bmatrix} \dfrac{E}{1-\nu^2} & \dfrac{\nu E}{1-\nu^2} & 0 & 0 & 0 & 0 \\[2mm] \dfrac{\nu E}{1-\nu^2} & \dfrac{E}{1-\nu^2} & 0 & 0 & 0 & 0 \\[2mm] 0 & 0 & E & 0 & 0 & 0 \\[2mm] 0 & 0 & 0 & G & 0 & 0 \\[2mm] 0 & 0 & 0 & 0 & G & 0 \\[2mm] 0 & 0 & 0 & 0 & 0 & G \end{bmatrix} \tag{31}
$$

Note that if the third row and third column of the matrix in Eq. (31) are eliminated, the resulting 5x5 matrix of elastic coefficients is exactly the same as the one used for degenerate solid shell elements.

Chapter 5

NUMERICAL TESTS

Several plate and shell benchmark problems were solved to test the
performance of the eighteen-node element based on the new mixed
formulation. For each problem, the results using the NMS18A and NMS18B
formulation are compared to the results for the eighteen-node assumed
displacement element (designated DISP18). Results for the NMS18C model
are included for only the ring problem which demonstrates that this
model locks for increasing radius to thickness ratios. Results using
the three-dimensional and modified stress-strain relations are compared
for plate and ring displacement problems. In addition, analytical or
other independent solutions are presented if available. All
computations were done in double precision Fortran on the UNIVAC
1100/92 machine at the University of Maryland.

5.1   Simply Supported and Clamped Square Plates

A square flat plate under uniform pressure is a good starting point
for testing any finite element that is to be used for shell analysis.
Effects of element geometry, boundary conditions and length to
thickness (L/t) ratios can easily be compared to analytical solutions.
In addition, the performance of the $\underset{\sim}{C}$ and $\underset{\sim}{C}_m$ matrices is easily tested.
The deflections of a square plate with simply supported and clamped
edges were calculated using uniform and distorted meshes. Due to
symmetry only one quarter of the plate is modeled. Typical elastic
properties for aluminum, $E = 10^7$ psi and $\nu = 0.3$, are used.

22

Evenly divided 2x2, 3x3 and 4x4 uniform meshes were used for both cases. Distorted 2x2 and 4x4 meshes were adequate for the simply supported plate, but 3x3 and 6x6 distorted meshes were also used for the clamped plate to check convergence. The 6x6 distorted mesh is formed by bisecting each element edge in the 3x3 distorted mesh. Figures 2a and 2b depict the four distorted meshes. Results for L/t ratios of 10^2, 10^3 and 10^4 are presented.

Normalized maximum deflections for uniform meshes are in Tables 1 and 2; distorted mesh results are in Tables 3 and 4. In each case the maximum deflection at the centroid of the plate is normalized with respect to the analytical solution obtained from thin plate theory [20,21]. The NMS18A and NMS18B formulations give numerical results that are very close to the analytical solution over a wide range of L/t ratios when uniform meshes and the modified stress-strain relation are used. NMS18C results are not reported, since for plate bending NMS18C is essentially the same as NMS18B. This is because the two models differ only in inplane strain terms and there is no inplane locking for the plate problem. When the regular stress-strain relation is used, results range from 17 to 20 percent below the analytical solution. This is due to normal strain locking, the inability of the element to represent accurately the condition of zero normal strain. Results for the simply supported plate with distorted meshes and the modified stress-strain relation are very good. The clamped plate is more sensitive to distorted meshes than the simply supported plate. However, when the distorted mesh size is increased to 6x6, results for the clamped plate with the modified stress-strain relation show good

23

agreement with the analytical solution. Even when $L/t = 10^4$, which is beyond the practical range, the solution differs by less than 2.5% from the analytical solution. The new mixed formulation performed better than the assumed displacment element in every case. The assumed displacement formulation element is extremely sensitive to increasing L/t ratio and distorted element geometry. Finally, it should be noted that for the plate problems, the NMS18A and NMS18B elements give virtually identical answers.

Table 5 lists the nondimensional bending moments for a 4x4 uniform regular mesh evaluated at the integration point nearest to the centroid of the plate. The computed values are normalized with respect to the analytical solution at the plate centroid using thin plate theory [19,20,21]. Although the sampling point is not exactly at the centroid, the results are insensitive to changing L/t ratio. This indicates that for the plate case the new mixed formulation elements are reliable for stress analysis.

5.2   Pinched Circular Ring

As shown in Figure 3, a circular ring is pinched by a concentrated load P at opposite points on the ring. Due to symmetry only one quarter of the ring was modeled with meshes of 4, 8 and 16 equally divided elements. Material and geometric properties are $E = 10^7$ psi, $v = 0.3$ and $R/t = 60, 100, 500$.

Table 6 lists the nondimensional displacement at the load point normalized to the analytical solution [5] for the NMS18A, NMS18B and NMS18C versions using the regular and modified stress-strain

24

relationships. No results for the assumed displacement model are shown. This is because the global stiffness matrices resulting from the assumed displacement formulation were ill-conditioned and could not be solved using a Cholesky decomposition scheme. The NMS18A and NMS18B formulations give accurate results for all mesh sizes when the modified stress-strain relation used. The results for the NMS18A and NMS18B models converge to a value about 9.5% below the analytical solution when the regular stress-strain relation is used. NMS18C exhibits locking as the R/t ratio increases. In addition, it performs more poorly than NMS18A or NMS18B for the 4 and 8 element meshes.

5.3 Pinched Cylindrical Shell

5.3.1 Diaphragmed Ends

A pinched cylindrical shell with diaphragmed ends is a good deep shell test problem since an analytical solution is available for comparison. The cylinder is pinched by a concentrated load P at two opposing points on the circle at the midsection. Due to symmetry and loading only one octant of the cylinder was modeled (Figure 4). Uniform and refined 4x6, 5x7, 6x8 and 7x9 meshes were used. The 4x6F (refined) mesh is formed by dividing the elements along lines BC and CD of a 3x5 (uniform) mesh. The 3x5 and 4x6F meshes are shown in Figure 5. The meshes illustrated in Figure 5 are on the stretched plane of octant ABCD of the cylinder. Refined meshes are more effective in modeling the steep gradients of deflections and stresses near the con-concentrated load. Material and geometric properties are $E = 1.05 \times 10^7$ psi, $\nu = 0.3$, $R = 4.953$ in., $L = 2R$ and $R/t = 100, 500$.

25

Tables 7 and 8 list the nondimensional displacement $\overline{W}_c = -W_c Et/P$ at the load point for the DISP18, NMS18A and NMS18B models with the modified stress-strain relation. Results using the regular stress-strain relation are not reported since the plate and ring problems demonstrate that when it is used locking occurs. Since the NMS18C formulation performed poorly on the ring problem no further results for it are reported.

Analytical solutions were calculated using 100 terms in each direction for the double Fourier series expression given by Flügge [22] and reported in Reference 19. For comparison, the results for a new mixed formulation degenerate solid shell element are reported. The element is the SHEL9N element that was first investigated by Rhiu [19] and examined in further detail in References 12 and 18. The SHEL9N element has nine nodes with three displacement and two rotational degrees of freedom at each node. Therefore, SHEL9N has 45 degrees of freedom versus 54 for the present eighteen-node solid elements.

Once again, the assumed displacement model performs poorly, especially for the larger R/t ratios. For R/t = 100, both the NMS18A and NMS18B results are close to the analytical solution and compare favorably with SHEL9N. When the R/t = 500 case is examined, it becomes clearer that the NMS18B formulation is superior to the NMS18A formulation. In fact, the NMS18B results are virtually identical to the SHEL9N answers.

5.3.2 Clamped Ends

For this test case the cylinder of the previous example is used,

26

but the ends are clamped instead of diaphragmed. Results for two

degenerate solid shell elements, one a triangular element [2] and the

other a nine-node element based on a conventional mixed formulation

[15], are presented for comparison. Nondimensional deflections at the

load point C are listed in Tables 9 and 10 for R/t = 100 and 500,

respectively. As before, the assumed displacement element performs

poorly. And once again, while answers for NMS18A and NMS18B are very

close at R/t = 100, NMS18B is much better at R/t = 500. In addition,

Figures 6 and 7 show inplane force N_x and moment M_y per unit length

along line BC for a 9x7 mesh with NMS18B elements. The results in

Figures 6 and 7 show excellent agreement with reference 4. The finite

element used in reference 4 is an accurate, cubic degenerate solid

shell element. Results for this element are not shown to avoid

cluttering.

5.4   Hemisphere under Alternating Point Loads

A hemishpere under directionally alternating point loads at the

free edge is shown in Figure 8. Due to symmetry only one quarter of

the hemisphere was modeled. In order to use only eighteen-node

elements, a 0.1° cutout was made at the pole and inplane displacements

along the resulting edge were constrained to zero. Both uniform and

refined 4x5, 5x6, 6x7 and 7x8 meshes were used. For the uniform meshes

each element subtends equal angles in the longitude (ϕ) and colatitude

(θ) directions. For a refined mesh the row of elements nearest the

pole are divided equally in the colatitude direction. In this way a

4x5F (refined) mesh is formed from a 4x4 uniform mesh. Figure 8 shows

27

a 4x4 uniform mesh divided to form a 4x5 mesh. For convenience the cutout is made after the mesh is formed. Material and geometric constants are $E = 10^7$ psi, $\nu = 0.3$, $R = 10$ in., $P = 2$ and $R/t = 250$, 500.

Nondimensional displacement $\overline{W}_A = DW_A/PR^2$ at point A is reported in Tables 11 and 12 for $R/t = 250$ and 500, respectively. The symbol D represents bending rigidity. As expected, the assumed displacement model performs poorly. For $R/t = 250$, NMS18B converges more quickly and both NMS18A and NMS18B give answers close to Morley's analytical solution [23]. Morley did not consider the $R/t = 500$ case, but a converged finite element solution using a sixteen-node element similar to SHEL9N is presented for comparison. Results for the three formulations are very close.

Chapter 6

CONCLUSIONS

The numerical tests demonstrate that the NMS18A and NMS18B mixed
formulation elements with the modified stress-strain relation give
reliable solutions for thin plate and shell problems. In the present
formulation, the assumed strain in conjunction with the modified
stress-strain relation effectively eliminates inplane, shear and normal
strain locking. Overall, the NMS18B version performed better than the
NMS18A version, thereby supporting the proposal that higher order
strain terms with a thickness coordinate are less likely to reintroduce
locking than other terms. Both the NMS18A and NMS18B formulations are
kinematically unstable at the element level, but are stable when two or
more elements are assembled. The NMS18C formulation, although kinema-
tically stable at the element level, performed poorly for curved
geometries. Thus, a judiciously chosen higher order strain has
successfully suppressed compatible kinematic modes without
reintroducing the locking effect. Finally, the kinematics of
deformation are more easily described with the eighteen-node solid
element than a degenerate solid shell element. Therefore, to make the
most of this advantage, the present formulation should be extended to
geometrically and materially nonlinear problems.
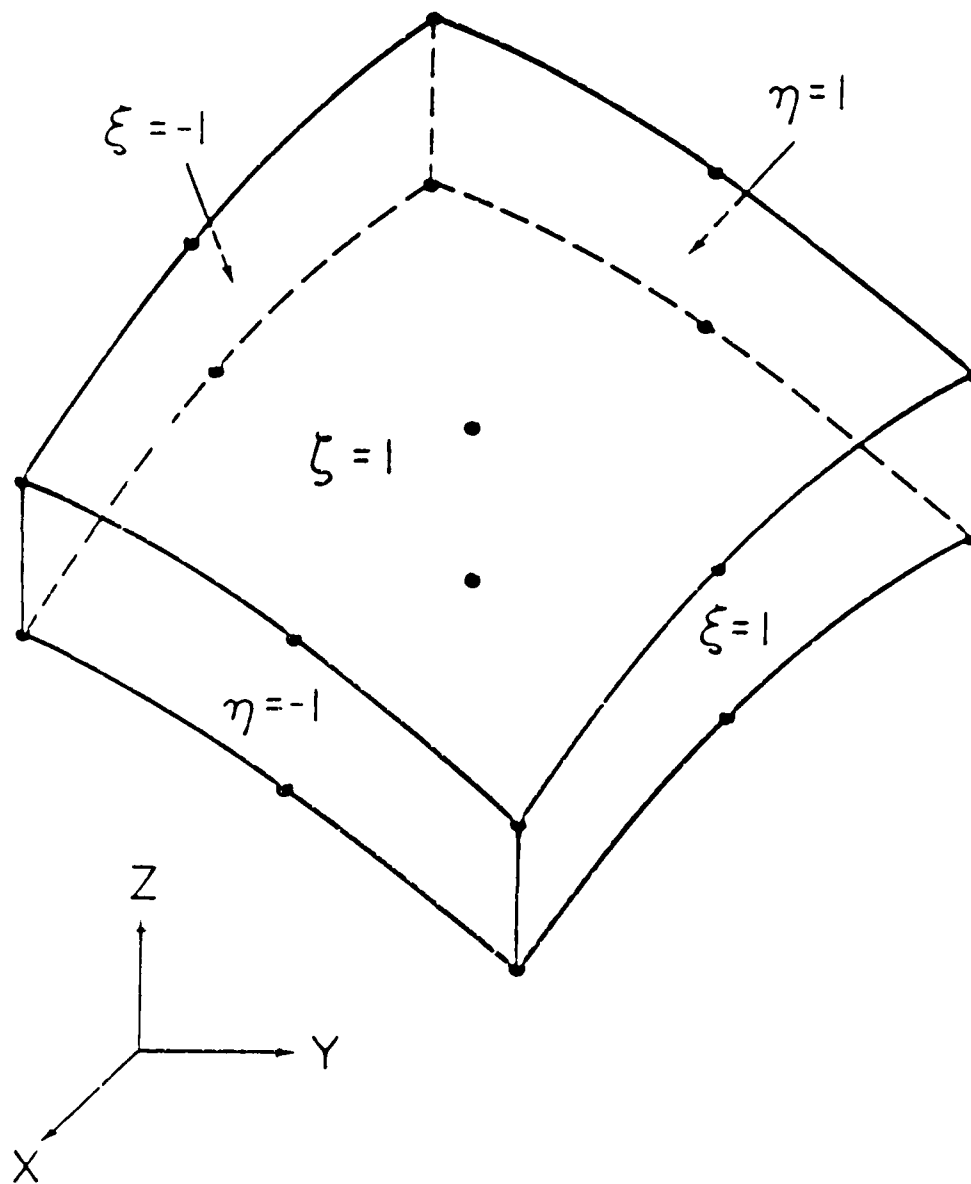
Figure 1   Eighteen-node element

30
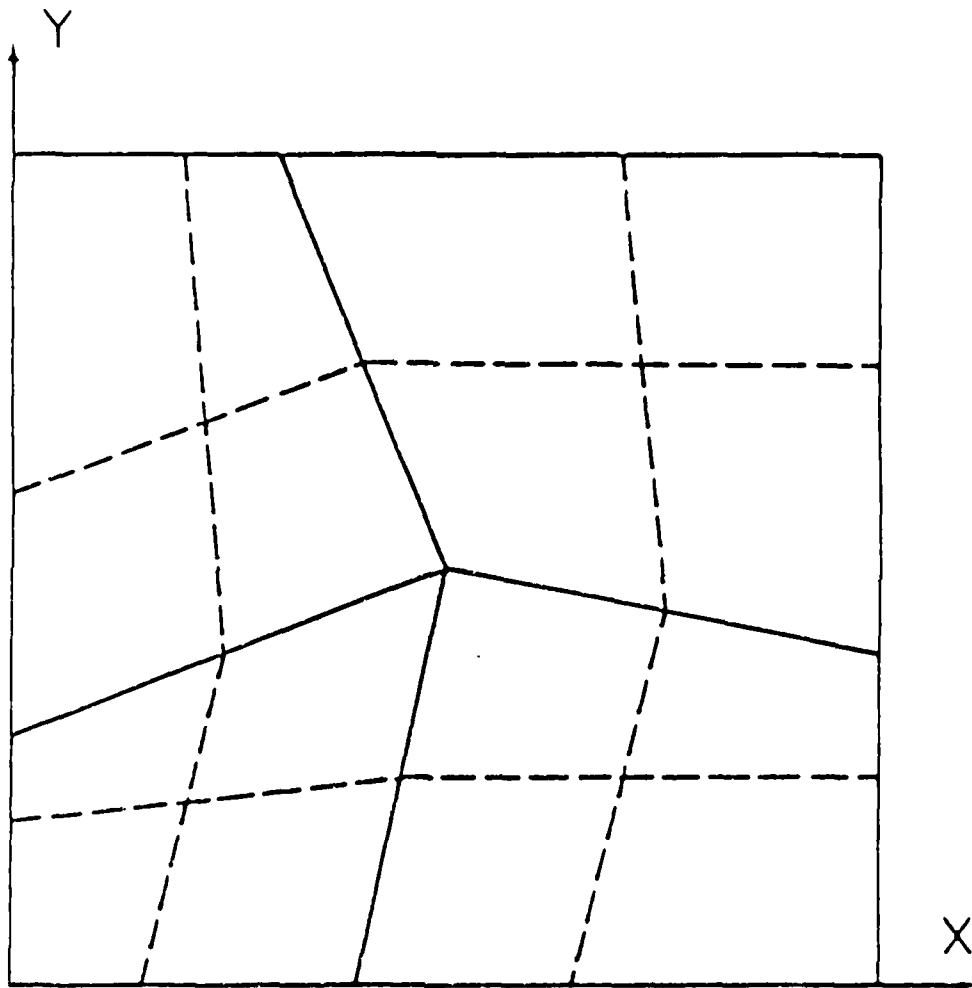
Figure 2a   Distorted 2x2 and 4x4 mexhes for one quarter
of a square plate
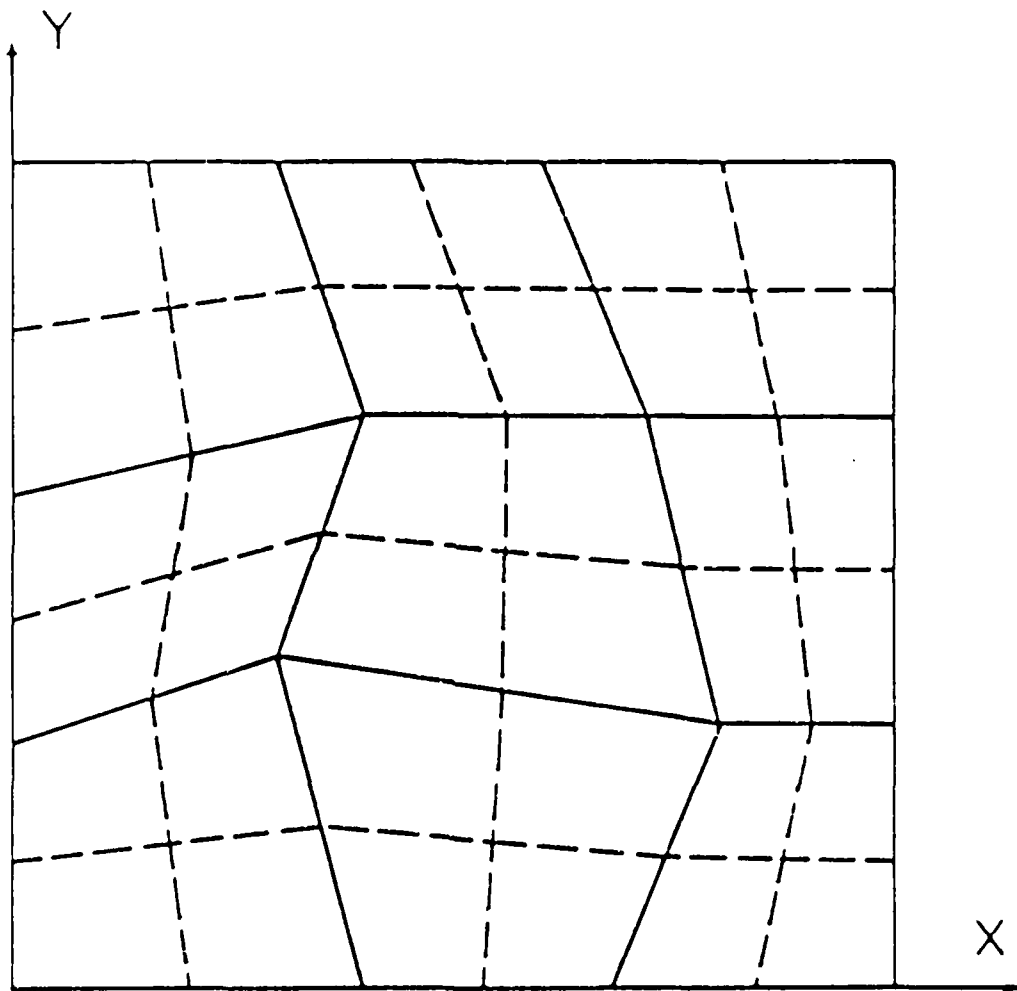
Figure 2b Distorted 3x3 and 6x6 meshes for one quarter
of a square plate
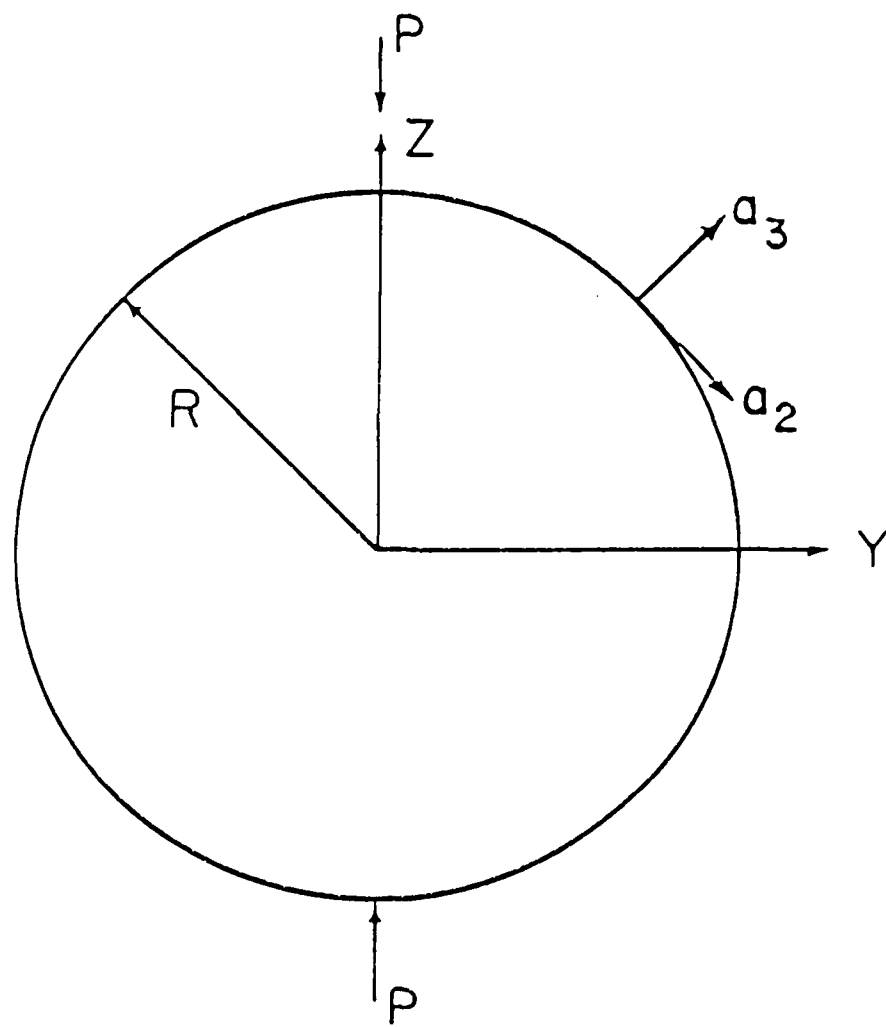
$R = 1.0$ in

$R/t = 60, 100, 500$

$E = 10^7$ psi

$\nu = 0.3$

$P = 1.0$

Figure 3   Pinched circular ring

33
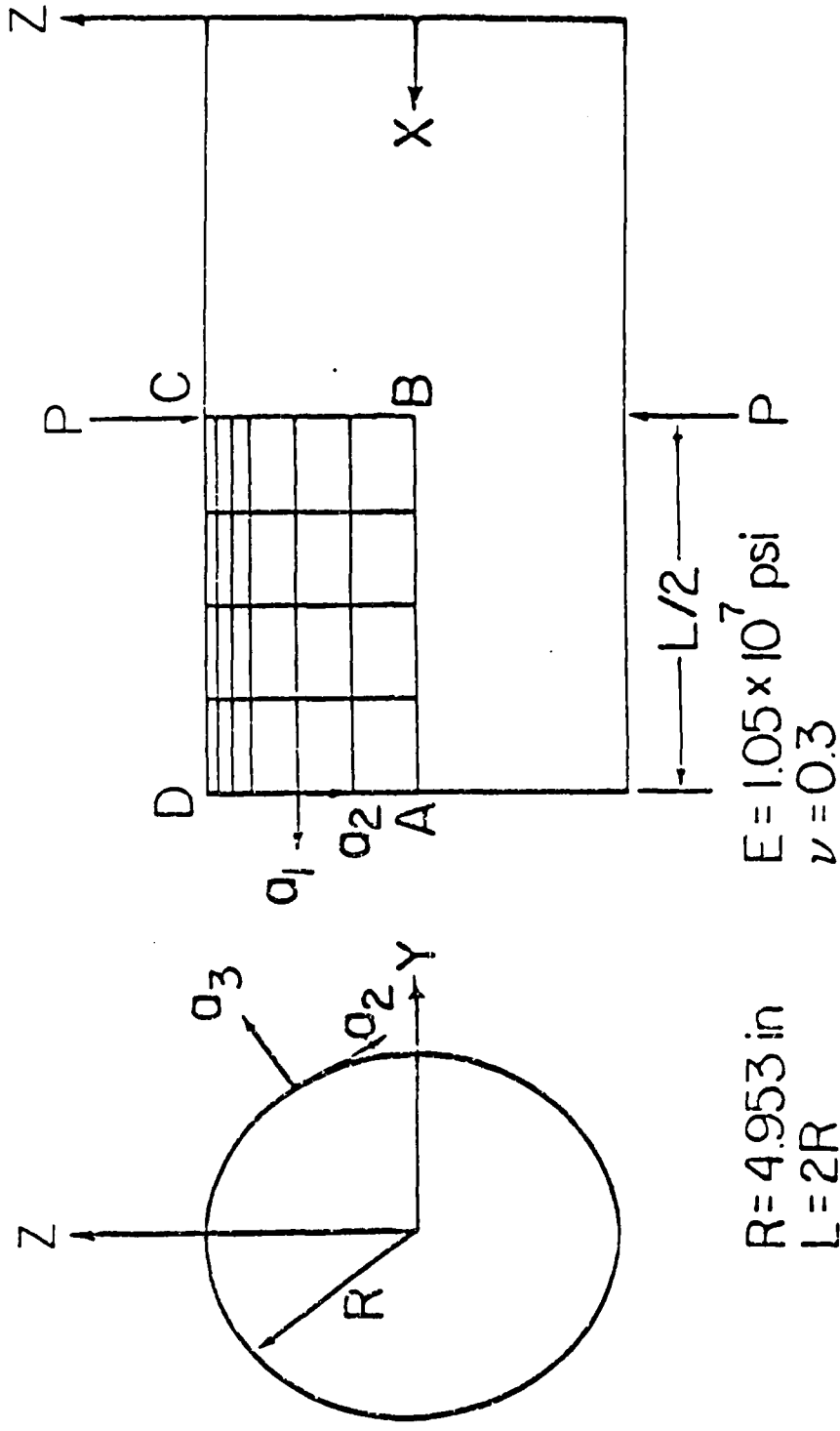
Figure 4 Pinched cylindrical shell

$E = 1.05 \times 10^7$ psi
$\nu = 0.3$

$R = 4.953$ in
$L = 2R$
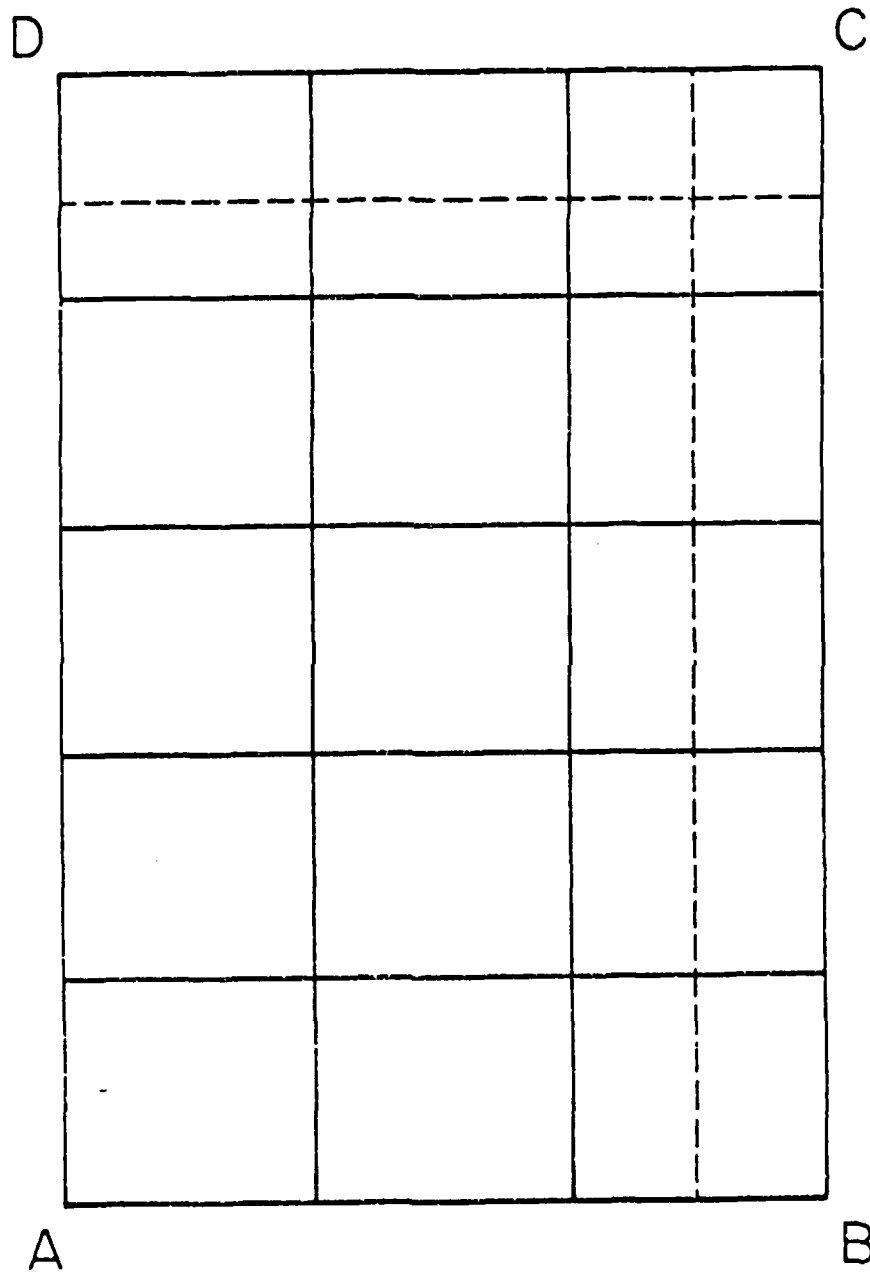
Figure 5   Uniform 3x5 and refined 4x6F meshes for cylindrical
           shell on the stretched plane of octant ABCD

35
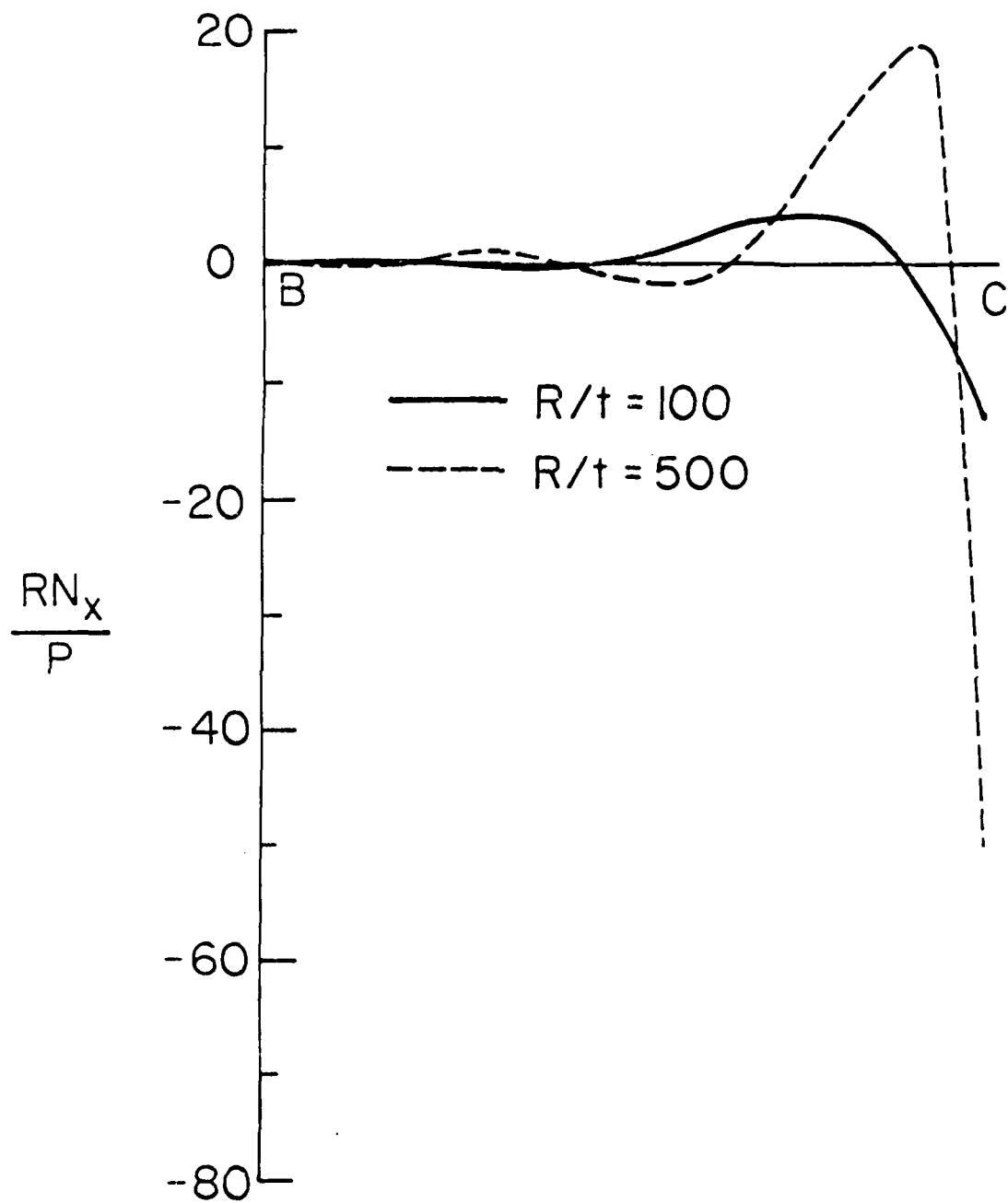
Figure 6 Nondimensional inplane force N_x per unit length along line BC
for cylindrical shell with fixed ends
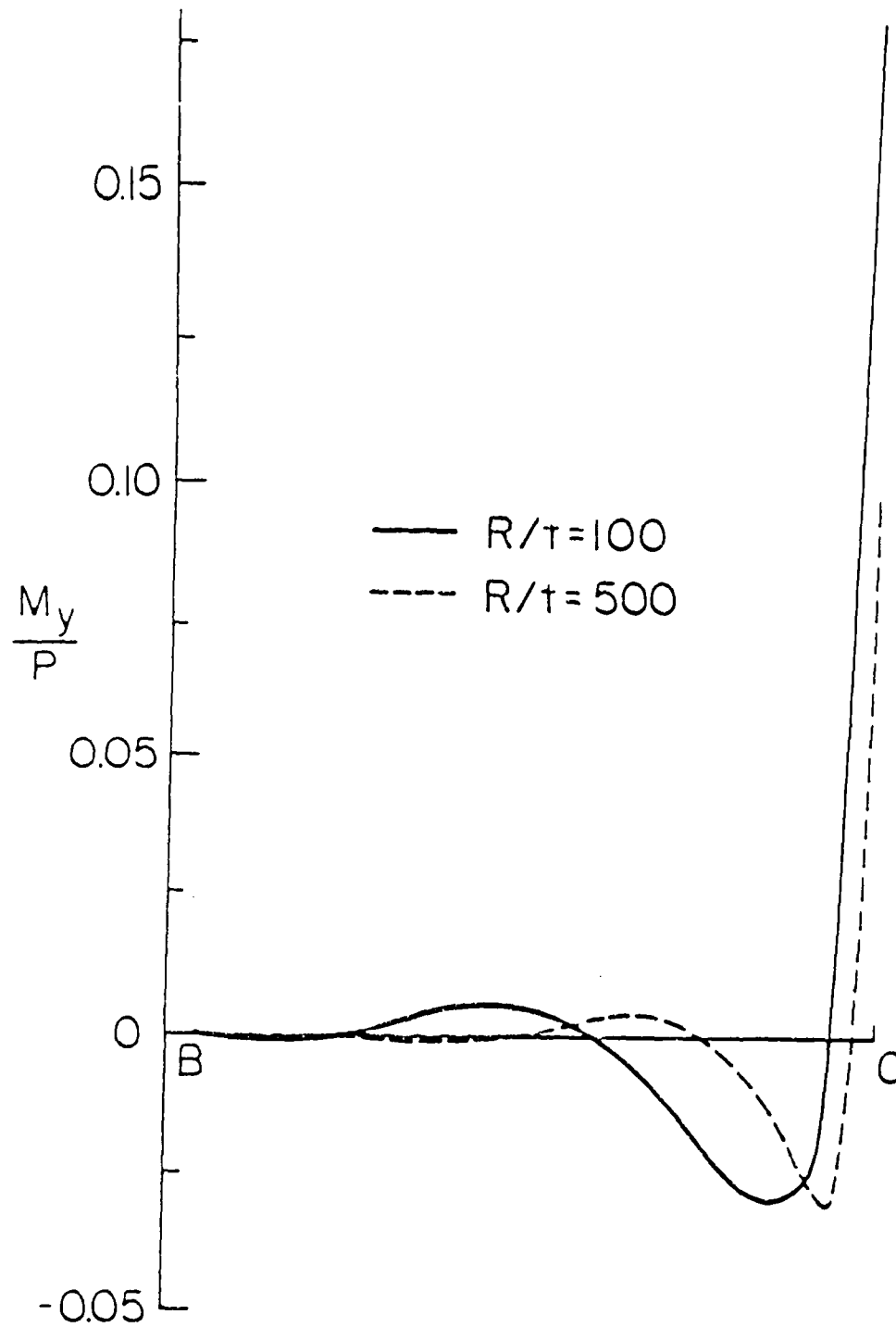
Figure 7   Nondimensional moment M_y along line BC for cylindrical shell with fixed ends

37

$R = 10.0$ in.

$R/t = 250,500$

$E = 10^7$ psi

$\nu = 0.3$

$P = 2.0$
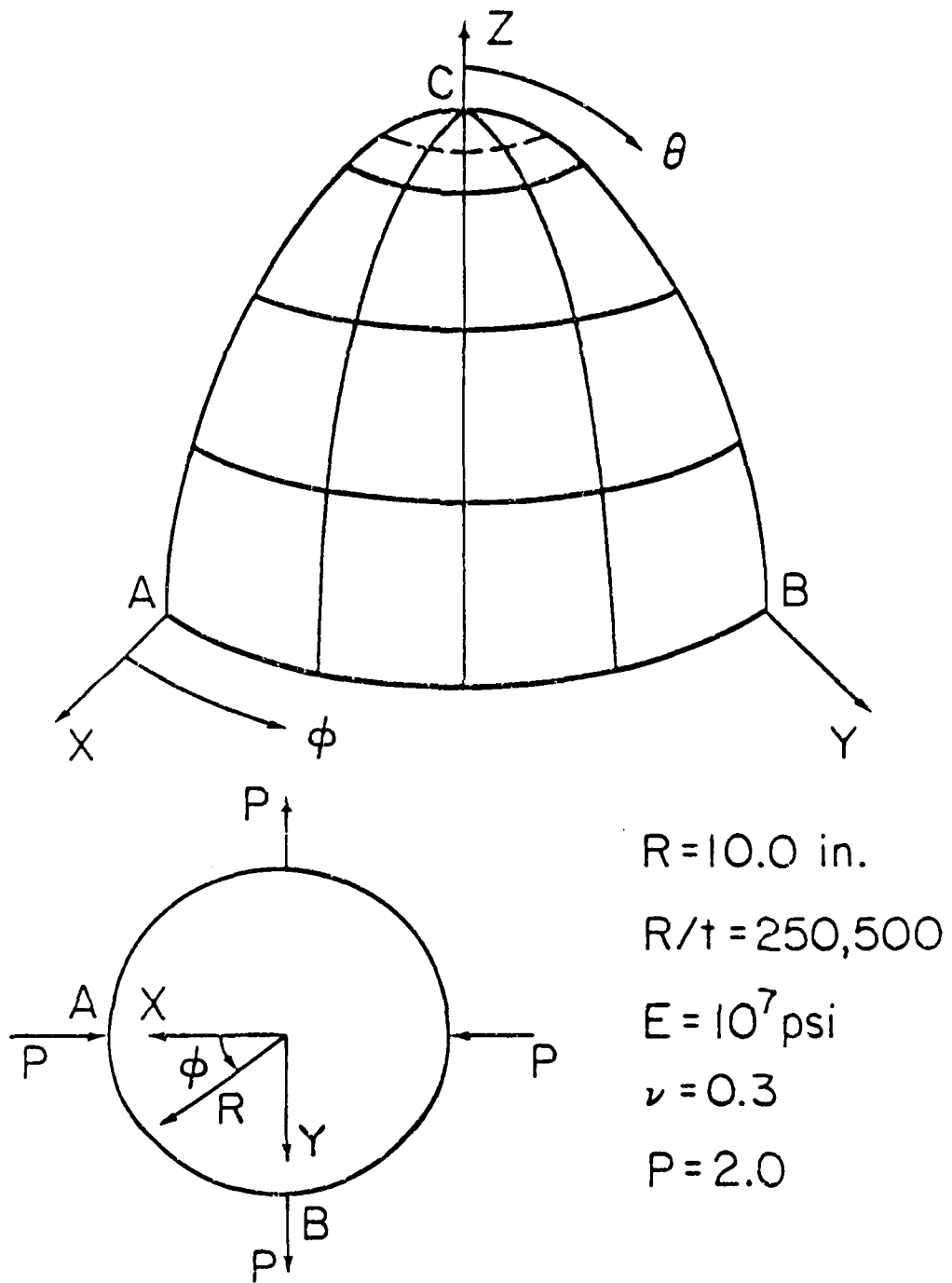
Figure 8   Hemisphere under alternating loads at the free edge

38

Table 1

Normalized maximum deflection of a simply supported square plate

under uniform pressure (regular meshes)

L/t	Type	2x2		3x3		4x4	
		$\underset{\sim}{c}$	$\underset{\sim}{c_m}$	$\underset{\sim}{c}$	$\underset{\sim}{c_m}$	$\underset{\sim}{c}$	$\underset{\sim}{c_m}$
	DISP18	.7815	.9573	.8024	.9830	.8095	.9918
10^2	NMS18A	.8145	1.0031	.8170	1.0033	.8183	1.0040
	NMS18B	.8145	1.0031	.8169	1.0033	.8183	1.0041
	DISP18	.7802	.9557	.8008	.9810	.8077	.9895
10^3	NMS18A	.8135	1.0018	.8153	1.0012	.8159	1.0008
	NMS18B	.8135	1.0018	.8153	1.0012	.8159	1.0008
	DISP18	.7850	.9585	.8034	.9846	.8099	.9919
10^4	NMS18A	.8135	1.0013	.8143	1.0003	.8147	.9986
	NMS18B	.8134	1.0013	.8143	1.0006	.8148	.9992

Table 2

Normalized maximum deflection of a clamped square plate

under uniform pressure (regular meshes)

L/t	Type	2x2		3x3		4x4	
		$\underset{\sim}{c}$	$\underset{\sim}{c}_m$	$\underset{\sim}{c}$	$\underset{\sim}{c}_m$	$\underset{\sim}{c}$	$\underset{\sim}{c}_m$
	DISP18	.6643	.7877	.7427	.9084	.7775	.9511
10^2	NMS18A	.8271	1.0129	.8200	1.0041	.8188	1.0026
	NMS18B	.8271	1.0129	.8200	1.0041	.8188	1.0026
	DISP18	.6373	.7807	.7362	.9018	.7712	.9448
10^3	NMS18A	.8254	1.0111	.8183	1.0024	.8171	1.0009
	NMS18B	.8254	1.0111	.8183	1.0024	.8171	1.0009
	DISP18	.6383	.7812	.7368	.9027	.7718	.9454
10^4	NMS18A	.8255	1.0111	.8179	1.0022	.8168	1.0004
	NMS18B	.8255	1.0112	.8180	1.0023	.8168	1.0005

Table 3

Normalized maximum deflection of a simply supported square plate
under uniform pressure (distorted meshes)

L/t	Type	2x2	4x4
10^2	DISP18	.9515	.9930
	NMS18A	1.0260	1.0129
	NMS18B	1.0260	1.0129
10^3	DISP18	.8757	.9670
	NMS18A	1.0236	1.0089
	NMS18B	1.0236	1.0089
10^4	DISP18	.1690	.5119
	NMS18A	1.0234	1.0059
	NMS18B	1.0235	1.0061

Table 4

Normalized maximum deflection of a clamped square plate under
uniform pressure (distorted meshes)

L/t	Type	2x2	3x3	4x4	6x6
10^2	DISP18	.5666	.8394	.9046	.9727
	NMS18A	.9432	.9914	1.0062	1.0003
	NMS18B	.9432	.9914	1.0062	1.0003
10^3	DISP18	.0625	.1648	.6838	.9340
	NMS18A	.6117	.8978	.9551	.9935
	NMS18B	.6117	.8978	.9551	.9935
10^4	DISP18	.0007	.0020	.0433	.3815
	NMS18A	.3623	.8414	.8978	.9771
	NMS18B	.3623	.8415	.8977	.9772

Table 5

Bending moment Mx at integration point nearest to the centroid
of a square plate normalized to the analytical solution at the centroid
(uniform 4x4 mesh)

	Simply Supported Plate		Clamped Plate	
L/t	NMS18A	NMS18B	NMS18A	NMS18B
10^2	.9982	.9982	.9909	.9909
10^3	.9961	.9961	.9907	.9907
10^4	.9938	.9944	.9901	.9903

Table 6

Maximum deflection at load point for a pinched circular ring

(normalized to analytical solution)

R/t	Type	4 elements		8 elements		16 elements	
		$\underset{\sim}{c}$	$\underset{\sim}{c}_m$	$\underset{\sim}{c}$	$\underset{\sim}{c}_m$	$\underset{\sim}{c}$	$\underset{\sim}{c}_m$
	NMS18A	.8988	1.0016	.9157	1.0043	.9159	1.0046
60	NMS18B	.9145	1.0029	.9156	1.0042	.9158	1.0045
	NMS18C	.6801	.8940	.8958	.9895	.9127	.9998
	NMS18A	.8895	1.0009	.9153	1.0041	.9157	1.0044
100	NMS18B	.9142	1.0024	.9154	1.0040	.9156	1.0044
	NMS18C	.5426	.7648	.8688	.9648	.9106	.9920
	NMS18A	.8570	.9991	.9146	1.0035	.9154	1.0041
500	NMS18B	.9134	1.0008	.9152	1.0035	.9154	1.0041
	NMS18C	.2958	.1785	.7089	.5542	.8865	.8874

Table 7

Nondimensional deflection at point C ($\overline{W}_c = -W_c Et/P$) for a pinched

cylinder with diaphragmed ends (R/t = 100)

Type	DISP18		SHEL9N		NMS18A		NMS18B	
Mesh	Uniform	Refined	Uniform	Refined	Uniform	Refined	Uniform	Refined
4x6	54.90	89.50	164.3	--	162.4	164.0	163.4	164.1
5x7	72.52	106.3	164.5	--	163.5	164.5	163.9	164.5
6x8	88.8	120.2	165.0	165.5	164.1	164.8	164.2	164.7
7x9	102.8	131.3	165.2	165.7	164.5	165.0	164.5	164.9

Flügge [22] 164.3

45

Table 8

Nondimensional deflection at point C ($\overline{W}_c = -W_c Et/P$) for a pinched

cylinder with diaphragmed ends (R/t = 500)

Type	DISP18		SHEL9N		NMS18A		NMS18B	
Mesh	Uniform	Refined	Uniform	Refined	Uniform	Refined	Uniform	Refined
4x6	63.59	162.0	1142.1	--	1001.8	1156.7	1135.9	1200.0
5x7	92.98	236.1	1178.8	--	1093.5	1188.0	1174.2	1208.1
6x8	129.7	315.7	1199.0	1215.5	1147.0	1204.9	1195.6	1214.9
7x9	173.8	396.1	1209.5	1218.7	1177.1	1212.8	1207.0	1218.1

Flügge [22] 1223.4

46

Table 9

Nondimensional deflection at point C ($\overline{W}_C = -W_C Et/P$) for a

pinched cylinder with clamped ends (R/t = 100)

Type	DISP18		NMS18A		NMS18B	
Mesh	Uniform	Refined	Uniform	Refined	Uniform	Refined
4x6	43.02	74.75	134.3	135.7	135.1	135.8
5x7	57.24	88.18	135.4	136.3	135.7	136.2
6x8	70.66	99.29	136.0	136.7	136.0	136.5
7x9	82.29	108.3	136.4	136.9	136.3	136.7

Reference 2   137.01

Reference 15   136.81

47

Table 10

Nondimensional deflection at point C ($\overline{W}_C = -W_C Et/P$) for a
pinched cylinder with clamped ends (R/t = 500)

Type	DISP18		NMS18A		NMS18B	
Mesh	Uniform	Refined	Uniform	Refined	Uniform	Refined
4x6	49.37	136.0	784.2	932.1	894.5	963.4
5x7	72.59	201.8	859.4	946.4	928.6	964.0
6x8	101.5	271.4	906.0	958.4	949.4	967.7
7x9	135.3	338.5	933.1	966.1	960.6	971.0

Reference 2   963.93

Reference 15   960.88

Table 11

Nondimensional deflection at point A ($\overline{W}_A = DW_A/PR^2$) for a hemisphere
under alternating point loads (R/t = 250)

Type	DISP18		NMS18A		NMS18B	
Mesh	Regular	Refined	Regular	Refined	Regular	Refined
4x5	.0040	.0030	.1767	.1799	.1783	.1815
5x6	.0090	.0069	.1828	.1845	.1834	.1851
6x7	.0171	.0135	.1845	.1855	.1848	.1858
7x8	.0284	.0233	.1851	.1857	.1853	.1858

Morley [23]   .1848

Table 12

Nondimensional deflection at point A ($\overline{W}_A = DW_A/PR^2$) for a hemisphere

under alternating point loads (R/t = 500)

Type	DISP18		NMS18A		NMS18B	
Mesh	Regular	Refined	Regular	Refined	Regular	Refined
4x5	.0010	.0008	.1544	.1620	.1574	.1647
5x6	.0023	.0018	.1733	.1774	.1743	.1785
6x7	.0046	.0036	.1795	.1818	.1800	.1823
7x8	.0080	.0064	.1818	.1832	.1821	.1835

Reference 4   .182

REFERENCES

1. S. Ahmad, B.M. Irons and O.C. Zienkiewicz, "Analysis of Thick and Thin Shell Structures by Curved Elements," Int. J. Num. Meth. Engn., 2, 419-451 (1970).

2. S.W. Lee, C.C. Dai and C.H. Yeom, "A Triangular Finite Element for Thin Plates and Shells," Int. J. Num. Meth. Engng., 21, 1813-1831 (1985).

3. S.W. Lee, S.C. Wong and J.J. Rhiu, "Study of a Nine-Node Mixed Formulation Finite Element for Thin Plates and Shells," Computers and Structures, 21, 1325-1334, (1985).

4. J.J. Rhiu and S.W. Lee, "A Sixteen-Node Shell Element with a Matrix Stabilization Scheme," accepted for publication in Computational Mechanics (1987).

5. S.W. Lee and T.H.H. Pian, "Improvement of Plate and Shell Finite Element by Mixed Formulations," AIAA J., 16, 29-34 (1978).

6. O.C. Zienkiewicz, J. Too and R.L. Taylor, "Reducd Integration Technique in General Analysis of Plates and Shells," Int. J. Num. Meth. Engng., 3, 275-290 (1971).

7. T.J.R. Hughes, M. Cohen and M. Haroun, "Reduced and Selective Integration Techniques in the Finite Analysis of Plates," Nuclear Engng. Design, 46, 203-222 (1978).

8. E.D.L. Pugh, E. Hinton and O.C. Zienkiewicz, "A Study of Quadrilateral Plate Bending Elements with Reduced Integration," Int. J. Num. Meth. Engng., 12, 1059-1079 (1978).

9. H. Stolarski and T. Belytschko, "Membrane Locking and Reduced Integration for Curved Elements," J. of Applied Mechanics, 49, 172-176 (1982).

10. T.J.R. Hughes, R.L. Taylor and W. Kanoknukulchai, "A Simple and Efficient Finite Element for Plate Bending," Int. J. Num. Meth. Engng., 11, 1529-1543 (1977).

11. H. Parish, "A Critical Survey of the 9-Node Degenerated Shell Element with Special Emphasis on Thin Shell Application and Reduced Integration," Comp. Meths. Appl. Mech. Engng., 20, 323-350 (1979).

12. S.W. Lee and J.J. Rhiu, "A New Efficient Approach to the Formulation of Mixed Finite Element Models for Structural Analysis," Int. J. Num. Meth. Engng., 21, 1629-1641 (1986).

13. T. Belytschko, J.S.J. Ong and W.K. Liu, "A Consistent Control of Spurious Singular Modes in the 9-Node Lagrange Element for the Laplace and Mindlin Plate Equations," Comp. Meth. App. Mech. Engng., 44, 269-295 (1984).

14. T. Belytschko, W.K. Liu, J.S.J. Ong and D. Lam, "Implementation and Application of a 9-node Lagrangian Shell Element with Spurious Mode Control," Computers and Structures, 20, 121-128 (1985).

15. S.C. Wong, "A Nine Node Assumed Strain Finite Element Model for Analysis of Thin Shell Structures," Ph.D. dissertation, Dept. of Aero. Engng., University of Maryland, May 1985.

16. S.W. Lee, "Finite Element Methods for Reduction of Constraints and Creep Analysis," Ph.D. dissertation, Dept. Aero. and Astro., MIT, Feb. (1978).

17. D.S. Malkus and T.J.R. Hughes, "Mixed Finite Element Methods - Reduced and Selective Integration Techniques: A Unification of Concepts," Comp. Meths. Appl. Mech. Engng., 15, 63-81 (1978).

18. J.J. Rhiu and S.W. Lee, "A New Efficient Mixed Formulation for Thin Shell Finite Element Models," Int. J. Meth. Engng., 24, 581-604 (1987).

19. J.J. Rhiu, "A New and Efficient Formulation for Finite Element Analysis of Thin Shell Structures Undergoing Small and Large Deflection," Ph.D. dissertation, Dept. of Aero. Engng., University of Maryland, Aug. 1985.

20. S.P. Timoshenko and S. Woinowsky-Krieger, Theory of Plate and Shells, 2nd Ed., McGraw-Hill, New York, 1959.

21. R. Szilard, Theory and Analysis of Plates, Prentice Hall, New Jersey, 1979.

22. W. Flugge, Stresses in Shells, Springer-Verlag, Berlin, 1962.

23. L.S.D. Morley and A.S. Morris, "Conflict Between Finite Elements and Shell Theory," in Finite Elements in the Commercial Environment, J. Robinson (ed.), Vol. 2, Okehampton, U.K. (1978).